Clathrin Polymerization Is Not Required for Bulk-phase Endocytosis in Rat Fetal Fibroblasts

Philippe Cupers, Alex Veithen, Anna Kiss, Pierre Baudhuin, and Pierre J. Courtoy

Cell Biology Unit, University of Louvain Medical School & International Institute of Cellular and Molecular Pathology, 1200 Brussels, Belgium

Abstract. To assess the role of clathrin in the bulk endocytic flow of rat foetal fibroblasts, the rate of internalization of fluid-phase and membrane-lipid tracers were compared, under control conditions and after inhibition of endocytic clathrin-coated pit formation. After intracellular potassium depletion or upon cell transfer into 0.35 M NaCl, the rate of internalization of receptor-bound transferrin and the residual membrane area of plasmalemmal clathrin-coated pits and vesicles were similarly decreased by ~90%. In contrast, the initial rate (<5 min) of intracellular accumulation of the fluid-phase tracer HRP was not affected. Both in control and treated cells, the rate of HRP accumulation declined after ~5 min, and was twofold lower in treated cells, due to enhanced regurgitation. After correction for regurgitation, the endocytic rate constant was similar to measurements at shorter intervals and identical in control and treated cells. Similarly, the rate of internalization and the steady-state level of intracellular accumulation of two fluorescent lipid derivatives, 6-[*N*-(7-nitro-2,1,3-benzoxadiazol-4-yl)amino]hexanoylglucosylsphingosine (C6-NBD-GlcCer) and 1-[4-(trimethylamino)phenyl]-6-phenyl-hexa-1,3,5-triene (TMA-DPH), were not affected by potassium depletion, indicating that the endocytic membrane traffic was equally preserved. Finally, the size distribution of primary endocytic particles that were accessible to HRP within 15 s before glutaraldehyde fixation was also indistinguishable in control and potassium-depleted cells. The simplest explanation is that clathrin polymerization is necessary to concentrate receptor-bound ligands in primary endocytic vesicles, but superfluous to the basic endocytic machinery in rat foetal fibroblasts.

A large variety of transmembrane proteins are rapidly internalized by a clathrin-associated pathway (for review see 54). Interaction between a specific sequence of their cytoplasmic domain and the AP2 complex (26, 44) promotes a ~10-fold concentration into clathrin-coated pits, resulting in highly efficient endocytosis (17, 45, 55, 68). Other molecules, that do not apparently require a direct interaction with AP2 complex, are also internalized by the clathrin-associated pathway (32, 34, 37, 50). These studies, as well as quantitative analysis on bulk fluid and membrane endocytosis, led to the proposal that pinocytosis could be fully explained by clathrin-coated pits and vesicles (34).

However, two lines of evidence argue against this simple hypothesis (for reviews see 65, 69). First, fluid-phase endocytosis can be enhanced, independently of the clathrin-associated pathway, by the induction of macropinocytosis (2, 22, 27, 46). Second, a large body of evidence supports the existence of clathrin-independent pinocytosis, different from macropinocytosis. For example, some molecules appear to be excluded from coated pits and to be internalized through non-clathrin-coated pits and delivered to endosomes (8, 42, 47, 59).

Caveolae, the omega-shaped invaginations of the plasma membrane with a uniform diameter of ~50 nm, seemed an attractive candidate for clathrin-independent pinocytosis. These pits are devoid of a clathrin coat and are covered instead by caveolin/VIP21 (13, 48). However, caveolae have been assigned a function of potocytosis, which is conceptually different from endocytosis, since it does not apparently involve budding of surface pits into primary endocytic vesicles (53, for reviews see 1, 66).

Direct evidence for clathrin-independent pinocytosis, distinct from macropinocytosis or potocytosis, was provided using techniques blocking the clathrin-coated endocytic pathway, such as intracellular potassium depletion (30), incubation in an hypertonic medium (11) and cytosolic acidification (49). These controlled perturbations severely inhibit receptor-mediated endocytosis by clathrin-coated pits (9, 11, 14, 16, 25, 30–32, 37, 40, 41, 49, 50), but have little or no effect on the accumulation of fluid-phase or adsorptive endocytic tracers (11, 16, 32, 40, 41, 49). However, to what extent net accumulation of fluid-phase tracers provided accurate es-

Address all correspondence to Pr. P. J. Courtoy, Cell Biology Unit, University of Louvain Medical School & International Institute of Cellular and Molecular Pathology, Avenue Hippocrate, 75, 1200 Brussels, Belgium. Tel.: 32 3 7647541. Fax: 32 2 7647543.

timation of fluid-phase endocytosis was not entirely clear. Indeed, intracellular accumulation is the result of endocytosis and regurgitation into the extracellular medium (4, 5, 10, 57).

Evidence was also reported supporting the coexistence of clathrin-associated and clathrin-independent pathways in untreated HEp-2 cells, where only non-clathrin-coated endocytic structures remained detected after potassium depletion (16). The diameter of clathrin-independent endocytic vesicles was found to be very close to that of clathrin-coated vesicles (16) and tracers internalized by the two routes appeared to converge into the same endosomes (18, 59).

Whereas such studies clearly show that pinocytosis can proceed through clathrin-coated and non-clathrin-coated pits and vesicles, they do not address the respective contribution of these two pathways to the constitutive bulk fluid and membrane flow, especially in nontransformed cells. In the absence of a specific tracer of clathrin-independent pinocytosis, we decided to block the clathrin-associated pathway by two reversible perturbations, potassium depletion and hypertonicity, and to measure the residual endocytic activity in rat foetal fibroblasts. The use of two treatments seemed necessary to exclude trivial artifacts of either procedure. Exact biochemical measurements of the rates of fluid and membrane entry, corrected for regurgitation and recycling, would predict the surface/volume ratio and the abundance of the two types of primary endocytic vesicles, that could be searched by ultrastructural cytochemistry and morphometry. If the two perturbations would also affect the clathrin-independent pathway, the study was expected to provide some insights on its regulation. To our surprise, we found that fluid and membrane endocytosis and the size distribution of primary endocytic vesicles were indistinguishable in control and treated cells, indicating that clathrin polymerization is superfluous to the basic endocytic machinery in nontransformed rat foetal fibroblasts.

Materials and Methods

Cell Culture

Rat foetal fibroblasts were isolated as described by Tulkens et al. (61) and grown in culture medium made of DME (GIBCO BRL, Gaithersburg, MD), supplemented by 20 mM glucose, 4 mM glutamine, 10 mM $NaHCO_3$, 10 mM Hepes, 10 μg/ml streptomycin, 66 μg/ml penicillin, and 10% (vol/vol) FCS (GIBCO BRL). Cultures were expanded in 175-cm^2 flasks (Nunc, Roskilde, Denmark) at 37°C, under 8% CO_2 in an humidified incubator. For the experiments, cells were detached by 5 mM EDTA in PBS (137 mM NaCl, 2.7 mM KCl, 8 mM Na_2HPO_4, and 1.5 mM KH_2PO_4, pH 7.4), centrifuged for 10 min at 920 rpm (centrifuge GR 4.11, Jouan Inc., Winchester, PA), resuspended in culture medium and seeded on 9.6 cm^2 (biochemical experiments) or 78.5 cm^2 (morphological experiments) plastic Petri dishes (Nunc). All experiments were carried out the day following the second subculture, at near confluency. Results summarized in this paper compile data from seven primary isolates, without significant variation with time.

Potassium Depletion and Hypertonic Treatment

Control cells were rinsed once with PBS-Ca^{2+} (137 mM NaCl, 5.4 mM KCl, 0.34 mM Na_2HPO_4, 0.44 mM KH_2PO_4, 3.6 mM $CaCl_2$, and 0.74 mM $MgSO_4$) and then incubated into the simplified medium described by Madshus et al. (31) (140 mM NaCl, 10 mM KCl, 1 mM $CaCl_2$, 1 mM $MgCl_2$, 20 mM Hepes, 5.5 mM glucose, and 1% (vol/vol) BSA, pH 7.4). The rate of transferrin endocytosis was identical with 5 or 10 mM KCl.

Potassium depletion was performed according to Madshus et al. (31, 32). Cells were rinsed once with PBS-Ca^{2+} and submitted to a 5-min hypotonic shock in DME/H_2O (1:1) at 37°C. Cells were then rapidly rinsed once with simplified medium devoid of KCl and incubated in this medium for 1 h at 37°C, before addition of endocytic tracers. As assayed by flame spectrophotometry, this technique led to a ~96% loss of intracellular potassium, that was fully reversible.

For hypertonic treatment, cells were rinsed once with PBS-Ca^{2+} and transferred in simplified medium, where final NaCl concentration was brought to 350 mM 20 min before addition of endocytic tracers. All subsequent incubations and washings were also performed in 350 mM NaCl.

Lactate dehydrogenase was assayed as described by Bergmeyr and Bernt (3). Cell volume and pH were measured by equilibration with ^{14}C-urea and partition with ^{14}C-benzoic acid, respectively (9, 31).

Receptor-mediated Endocytosis of Transferrin

Iron-saturated transferrin (Sigma Chem. Co., St. Louis, MO) was labeled by ^{125}I iodine (100 mCi/ml; Amersham Corp., Arlington Heights, IL) as described by McFarlane (33), to a specific radioactivity of 700-1000 cpm/ng of protein. Control, potassium-depleted or NaCl-treated cells (~45,000/cm^2 dish) were incubated at 37°C in the appropriate simplified medium (normal, without KCl or hypertonic) containing 50 nM ^{125}I-transferrin, rapidly cooled down to 4°C (by dipping dishes into ice-cold PBS-Ca^{2+}), washed five times with PBS-Ca^{2+}, surface digested for 1 h with 0.3% (wt/vol) pronase (Boehringer Mannheim Corp., Indianapolis, IN) in DME, and pelleted with a table microfuge (Beckman Instrs., Carlsbad, CA) for 1 min at 4°C. The supernatant was recovered and the pellet was finally washed directly twice with PBS-Ca^{2+} and lysed in 0.01% (vol/vol) Triton X-100 (Serva Biochemicals, Paramus, NJ). The pronase-resistant fraction, corresponding to the cell pellet, was taken as a measure of intracellular transferrin and was assayed for protein and radioactivity; the supernatant, containing the pronase-sensitive fraction, was considered as cell surface-bound transferrin and was assayed for radioactivity. This technique released 98% of ^{125}I-transferrin that could bind to the cell surface at 4°C. Proteins were measured according to Lowry, using BSA as a standard. ^{125}I radioactivity was determined using a gamma counter (1275 Minigamma; LKB Wallac, Sollentuna, Sweden).

Fluid-phase Endocytosis of HRP

Control, potassium-depleted or NaCl-treated cells were incubated at 37°C in the appropriate simplified medium (normal, without KCl or hypertonic) containing 1 to 10 mg/ml HRP (grade II; Boehringer Mannheim Corp.), for the indicated intervals. They were then transferred at 4°C and extensively washed: three times 30 s with simplified medium without BSA, once for 5 min and once for 1 min with simplified medium containing 10% outdated newborn calf serum (previously dialyzed against 155 mM NaCl), and finally five times 30 s with simplified medium without BSA. This extensive washing procedure allowed to remove essentially all HRP adsorbed to the cell surface, since incubation at 4°C with 2 mg/ml HRP, followed by extensive washings led to no detectable peroxidase activity (<1 ng/mg cell protein). Cells were finally lysed in 0.01% (vol/vol) Triton X-100 and scraped off with a rubber policeman. HRP activity in the lysate was measured by the stopped colorimetric assay using ortho-dianisidine as a substrate, according to Steinman et al. (56), and expressed with respect to the protein content.

For pulse-chase experiments, control, potassium-depleted or NaCl-treated cells were incubated at 37°C for various intervals in the appropriate medium containing 2-8 mg/ml HRP, washed as described above, and reincubated at 37°C in HRP-free medium, for the indicated intervals. Thereafter, cells were rapidly washed at 4°C three times 30 s with PBS-Ca^{2+}, lysed and assayed for HRP activity and protein content.

C6-NBD-GlcCer Endocytosis

Uptake and recycling of C6-[*N*-(7-nitro-2,1,3-benzoxadiazol-4-yl)amino]-hexanoylglucosylsphingosine (C6-NBD-GlcCer)[1], kindly provided by Professor D. Hoekstra (University of Groningen, The Netherlands) was per-

1. *Abbreviations used in this paper*: C6-NBD-GlcCer, 6-[*N*-(7-nitro-2,1,3-benzoxadiazol-4-yl)amino]hexanoylglucosylsphingosine; C6-NBD-SM, *N*-[N-(7-nitro-2,1,3-benzoxadiazol-4-yl)-ε-aminohexanoyl]-sphingosylphosphorylcholine; TMA-DPH, 1-[4-(trimethylamino)phenyl]-6-phenylhexa-1,3,5-triene.

formed as described by Kok et al. (28). Control or potassium-depleted cells were first incubated in the appropriate simplified medium at 37°C for 1 h, transferred at 4°C and washed three times with ice-cold 155 mM NaCl. They were then incubated at 4°C for 30 min in simplified medium without BSA, but containing 1 μM C6-NBD-GlcCer. Cells were washed five times with ice-cold 155 mM NaCl and reincubated at 37°C in the appropriate simplified medium without BSA for the indicated intervals. At the end of the pulse, cells were transferred again at 4°C, washed three times 30 s with PBS-Ca^{2+}, four times 15 min with PBS-Ca^{2+} containing 5% BSA (wt/vol) and 10 times 30 s with PBS-Ca^{2+} (back-exchange procedure). Finally, cells were lysed in 0.01% Triton X-100 and scraped with a rubber policeman. C6-NBD-GlcCer content was quantitated in a spectrofluorimeter (SFM25; Kontron Analytical, Milan, Italy) with excitation at 465 nm and emission at 530 nm, by reference to a known amount of C6-NBD-GlcCer. The back-exchange procedure released 94% of the labeling.

For recycling studies, C6-NBD-GlcCer was incorporated at 4°C, internalized for various intervals at 37°C, and back-exchanged at 4°C as described above. Cells were then reincubated in simplified medium at 37°C for the indicated periods of chase. After a second back-exchange, C6-NBD-GlcCer was quantitated in cell lysates as described above.

TMA-DPH Endocytosis

Internalization of 1-[4-(trimethylamino)phenyl]-6-phenylhexa-1,3,5-triene (TMA-DPH), kindly provided by Professor Kuhry (University of Strasbourg, France), was performed according to Illinger and Kuhry (24). Control or potassium-depleted cells were first incubated in the appropriate simplified medium at 37°C for 1 h, transferred at 4°C and washed three times with ice-cold 155 mM NaCl. They were surface-labeled by incubation in the appropriate simplified medium containing 2 μM TMA-DPH for 2 min at 4°C, then transferred to 37°C and incubated in the same prewarmed medium for the indicated intervals. At the end of the incubation, they were rapidly washed five times with PBS-Ca^{2+} at 4°C, carefully detached from the Petri dishes with a cell lifter (Costar) and immediately assayed for fluorescence with a fluorimeter (Perkin-Elmer 1000; The Perkin-Elmer Corp., Norwalk, CT), with excitation at 362 nm and emission at 435 nm.

The reversibility of the plasma membrane labeling with TMA-DPH was consistently more extensive than for C6-NBD-GlCer (98 versus 94%). Hence, measurements obtained after 5 min of tracer internalization with TMA-DPH should be considered as more accurate.

Electron Microscopy and Wicksell's Transformation

Control, potassium-depleted or NaCl-treated cells were rapidly rinsed with 155 mM NaCl, fixed by 2% (vol/vol) glutaraldehyde in 0.1 M sodium cacodylate buffer, pH 7.4, for 30 min at 4°C, and washed again three times for 10 min with 50 mM Tris-HCl, pH 6.0. Cells were postfixed with a 1% (wt/vol) OsO_4-2% $K_4Fe(CN)_6$ solution, stained en bloc with 1% uranyl acetate for 2 h and pelleted in 2% agar. Pellets were dehydrated in graded ethanol and embedded in Spurr. Ultrathin (50 nm nominal) sections were obtained with a Reichert ultramicrotome (Reichert, Wien, Austria), collected on rhodanium 400 mesh grids and contrasted with 3% uranyl acetate for 10 min, followed by lead citrate for 10 min. Grids were washed with water, dried, and examined in a Philips 301 electron microscope operating at 60 kV.

To characterize the population of endocytic clathrin-coated round pits and vesicles, the diameter of round-shaped bristle coated profiles in continuity with, or located at less than 1 μm from the sectioned cell surface, was measured from random pictures. Size distributions of profiles were submitted to the Wicksell's transformation on a PS 2/55SX (IBM), to estimate the corresponding distribution of particles in the fixed tissue. The abundance of particles per μm^3 of cell was also determined, so that total membrane area and volume of endocytic clathrin-coated compartment per μm^3 cell could be deduced on the basis of the average values of particles, not of profiles.

Peroxidase Cytochemistry and Size Distribution of HRP-labeled Endocytic Vesicles

For ultrastructural HRP cytochemistry, control or potassium-depleted cells were pulse-labeled at 37°C for 15–60 s with 8 mg/ml HRP (grade II; Boehringer Mannheim Corp.) in the appropriate simplified medium, immediately cooled down, washed as for biochemical studies, and fixed as described above. Peroxidase cytochemistry was then performed. Cells were washed three times for 10 min in 50 mM Tris-HCl, pH 6.0, preincubated in the dark for 15 min in the same buffer containing 2 mg/ml diaminobenzidine (Sigma Chem. Co.). This medium was prepared extemporaneously, adjusted to pH 6.0, supplemented with 25 mM thimerosal (Sigma Chem. Co.), and filtered through 0.22-μm pore filters (Millipore Corp., Bedford, MA). The addition of thimerosal was found to increase the ultrastructural contrast and to decrease the diffusion of the reaction product outside vesicles (Courtoy, P. J., manuscript in preparation). The cytochemical reaction was started by the addition of 0.02% (vol/vol) H_2O_2 and allowed to develop for 30 min in the dark. Cells were then rinsed three times for 10 min in 50 mM Tris-HCl, pH 6.0, postfixed for 1 h at 4°C in the osmium-ferrocyanide solution and processed for electron microscopy as described above. Sections were surveyed at the electron microscope and all HRP-labeled profiles were photographed. Micrographs were scanned (IBM scanner type 3119 S/N 97 and IBM PS/2 55 SX) and analyzed for size distribution of profiles, using Image 1.44 computer program (National Institutes of Health, public domain). Size distributions of particles were deduced by the Wicksell's transformation as above.

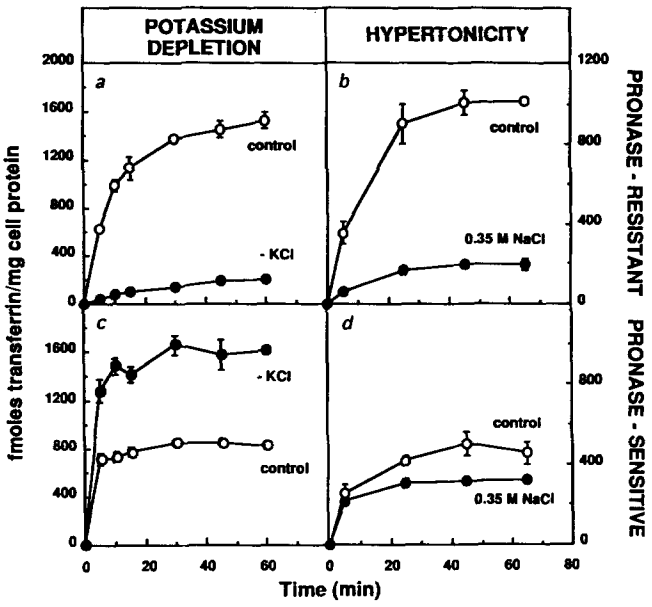

Figure 1. Effect of potassium depletion and hypertonicity on transferrin endocytosis. Control (*a–d, open circles*), potassium-depleted cells (*a* and *c, filled circles*) and NaCl-treated cells (*b* and *d, filled circles*) were incubated at 37°C for the indicated times in the corresponding simplified medium containing 50 nM ^{125}I-transferrin. They were washed five times with PBS-Ca^{2+} at 4°C, digested for 1 h with 0.3% pronase, pelleted, and lysed. Pronase-resistant fraction (*a* and *b*, intracellular transferrin) and pronase-sensitive fraction (*c* and *d*, cell surface-bound transferrin) are represented. The figure shows a representative experiment out of five; each value is the mean ±SD of three dishes.

Results

Receptor-mediated Endocytosis of Transferrin

Inhibition of the clathrin-dependent pinocytic pathway in rat fibroblasts by potassium depletion and by incubation in hypertonic medium was first examined following receptor-mediated endocytosis of transferrin.

Potassium depletion in simplified medium was effective after ~45 min and resulted in a 90% decrease of the subsequent intracellular accumulation of transferrin, while a two-fold increase of surface-bound transferrin was observed (Fig.

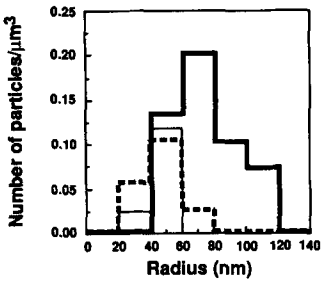

Figure 2. Effect of potassium depletion and hypertonicity on clathrin-coated compartment. Control (*thick line*), potassium-depleted cells (*dashed line*) and NaCl-treated cells (*thin line*) were washed with 155 mM NaCl, after 1-h treatment, and fixed with 2% glutaraldehyde in 0.1 M cacodylate buffer, pH 7.4. Round-shaped coated profiles were measured in random sections, and Wicksell's transformation was performed. This experiment was repeated once with similar results. Average values and other parameters from the same population are summarized at Table I.

Table I. Characterization of Peripheral Clathrin-coated Structures

	Control	−KCl*	0.35 M NaCl*
Biological sampling area (μm^2)	500	333	501
Number of measured profiles	47	8	9
Average particle parameters			
Radius (μm)	0.0745	0.0468	0.0466
Surface (μm^2)	0.0748	0.0296	0.0280
Volume (μm^3)	0.0021	0.0005	0.0004
Total compartment			
Number/μm^3 cell	0.5210	0.1887	0.1418
Membrane area ($\mu m^2/\mu m^3$ cell)	0.0390	0.0055	0.0040
Fractional volume (%)	0.1100	0.0100	0.0060

Same material and experimental protocol as for Fig. 2.
* Owing to the limited number of coated profiles in treated cells, data are obviously approximate.

1, *a* and *c*). Whether the rate of internalization of surface-bound transferrin was 0.12/min for control cells, it fell to ~0.01/min after potassium depletion. The actual inhibition of endocytosis of bound transferrin was thus ~95%. When cells were incubated in DME without KCl, instead of simplified medium without KCl, a similar level of potassium depletion (>95% loss) was observed, but surprisingly, transferrin internalization was not affected.

Hypertonic treatment was immediately effective (<5 min), causing a 80% decrease of intracellular transferrin accumulation and a slight decrease in transferrin binding after 5 min (Fig. 1, *b* and *d*). Thus, the two perturbations proved appropriate to severely inhibit receptor-mediated endocytosis, i.e., the clathrin-dependent endocytic pathway, in rat foetal fibroblasts. However, hypertonic treatment consistently resulted in some loss (10–15%) of cell protein, indicating that the procedure was less well tolerated than potassium depletion. Nevertheless, lactate dehydrogenase activity per mg cell protein remained unaffected and the effect of hypertonicity on ^{125}I-transferrin endocytosis, as for potassium depletion, was fully reversible. The cellular potassium content was not appreciably affected by hypertonicity. Neither potassium depletion, nor hypertonic treatment significantly altered cytosolic pH (control, 7.4 ± 0.1; potassium depletion, 7.3 ± 0.1; hypertonicity, 7.4 ± 0.1).

Morphometry of Endocytic Clathrin-coated Particles

To correlate the inhibition of receptor-mediated endocytosis of transferrin with ultrastructural alterations of clathrin-coated endocytic pits and vesicles, we surveyed the cell surface of control, potassium-depleted and NaCl-treated cells in random micrographs, and analyzed clathrin-coated profiles by morphometry. All structures covered with a typical bristle coat that were in continuity with the plasma membrane in the plane of the section or at <1 μm from the plasma membrane profile were considered as endocytic coated pits and vesicles. The actual average dimensions of clathrin-coated particles in glutaraldehyde-fixed cells were further computed from the observed size distribution of profiles by applying the Wicksell's transformation.

In control rat foetal fibroblasts, peripheral clathrin-coated particles, presumably endocytic, had an average radius of 74.5 nm (Fig. 2 and Table I). Their abundance was estimated at 0.52/μm^3 cell, corresponding to ~1555 particles/cell (the average volume of a rat foetal fibroblast, based on four independent determinations, was 2990 ± 150 μm^3).

The effect of potassium depletion and incubation in hypertonic medium on peripheral clathrin-coated particles were comparable: the average radius was decreased ~1.6-fold, while their abundance was reduced approximately threefold (Fig. 2 and Table I). As a consequence, the total area and the fractional volume of clathrin-coated endocytic structures in treated cells were reduced to 10–14% and 6–9% of controls, respectively. These estimates of the endocytic clathrin-coated area are in excellent agreement with the biochemical measurements of the inhibition of receptor-mediated endocytosis of transferrin. They further imply that the contribution of the clathrin-coated pathway to fluid pinocytosis would also be severely decreased. Hence, we measured the rate of fluid-phase endocytosis in control and treated cells.

Fluid-phase Endocytosis: HRP Accumulation

In our hands, horseradish peroxidase, combined with the extensive washing procedure described in Materials and Methods, did not result in detectable accumulation at 4°C and its uptake at 37°C yielded the best estimates of fluid-phase endocytosis in rat foetal fibroblasts. Indeed, its accumulation after 60 min uptake was proportional to the extracellular concentration between 0.5 and 16 mg/ml and consistently resulted in lower estimates than those observed for ^{3}H-sucrose, ^{3}H-inulin and much lower values than those found with ^{125}I-BSA (data not shown). Rat foetal fibroblasts do not have any detectable endogenous peroxidatic activity.

Accumulation of HRP in control and treated cells showed a rapid linear phase, followed after 5 min by a slower linear phase (Fig. 3). The decrease in the rate of HRP accumulation after 5 min is attributed to an intermediate compartment regurgitating its content. Direct evaluation of the rate of fluid-phase endocytosis was thus limited to pulses of 1–4 min, assuming that HRP regurgitation was negligible during this interval. Based on these short intervals of HRP uptake, clearance by fluid-phase endocytosis was estimated at 267 ± 44 nl/h/mg cell protein (n = 4; Table II).

In potassium-depleted cells, HRP accumulation was comparable (292 ± 59 nl/h/mg cell protein (n = 4) to that of control cells during short pulses (1–4 min), but decreased to 40 to 60% of control cells thereafter (Fig. 3, *a* and *b* and Table II). Similar observations were made after hypertonic treatment (Fig. 3, *c* and *d* and Table II), although the initial uptake was lower in treated than in control cells (198 ± 39

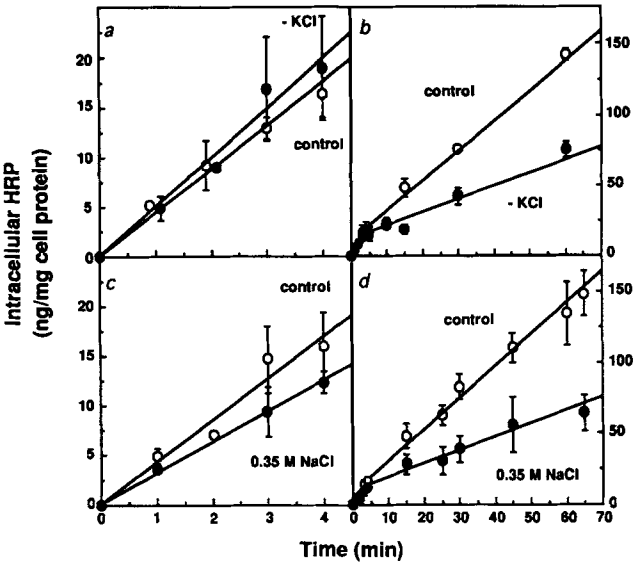

Figure 3. Effect of potassium depletion and hypertonicity on HRP accumulation. Control (*a–d, open circles*), potassium-depleted cells (*a* and *b, filled circles*) and NaCl-treated cells (*c* and *d, filled circles*) were incubated at 37°C in the corresponding simplified medium containing 2 to 8 mg/ml HRP. Cells were extensively washed at 4°C and lysed. Values have been normalized to an extracellular HRP concentration of 1 mg/ml. Left panels focus on short pulses (*a* and *c*, 1–4 min). Right panels focus on long pulses (*b* and *d*, 10–60 min). The slope after short pulses (1–4 min) provided a direct measurement of the rate of fluid-phase endocytosis (see Table II). Each value is the mean ±SD of 4 to 12 dishes, compiled from 2 to 4 experiments.

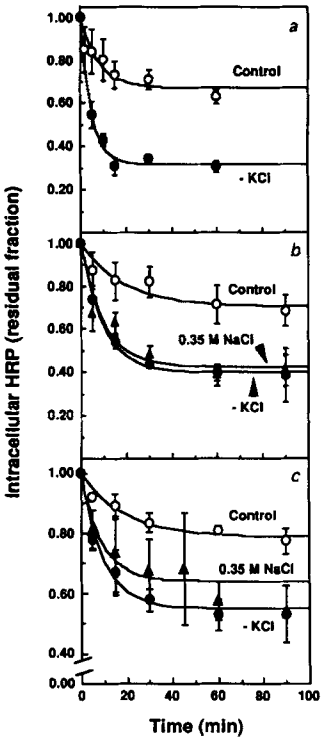

Figure 4. Effect of potassium depletion and hypertonicity on HRP regurgitation. Control (*open circles*), potassium-depleted (*filled circles*), and NaCl-treated cells (*filled triangles*) were incubated at 37°C in the corresponding simplified medium containing 2 to 8 mg/ml HRP for pulses of 5 min (*a*), 15 min (*b*), or 30 and 60 min (*c*). They were washed extensively at 4°C, reincubated at 37°C for the indicated times in the appropriate HRP-free medium, briefly washed again, and lysed. Results are expressed as residual fractions of HRP accumulated at the beginning of the chase, as a function of time of chase. In each condition, values were indistinguishable after pulses of 30 and 60 min and were pooled. On each graph, symbols represent means ±SD of one to three experiments (three to four samples each). Curves represent least squares fitting, according to equation A1 (see Appendix).

ng/h/mg cell protein). The effects of both perturbations on fluid-phase endocytosis were also fully reversible. A comparable initial rate of fluid-phase endocytosis followed by a lower accumulation suggested that the two treatments did not affect fluid-phase entry, but rather affected the partitioning of tracer between sequestrative and regurgitative pathways.

Fluid-phase Endocytosis: HRP Regurgitation

Regurgitation was measured using pulse-chase experiments. We performed pulses of 5 to 60 min in presence of HRP and results were expressed as the residual fraction of internalized tracer versus time of chase. For all conditions and times tested, regurgitation showed an exponential decay.

In control cells, the releasable HRP fraction reached 33% of accumulated tracer after a 5-min pulse (Fig. 4 *a*), 29% after a 15-min pulse (Fig. 4 *b*) and 22% after a 30- and 60-min (Fig. 4 *c*) or longer pulses (120–240 min, data not shown). This indicates that after filling of an early, readily regurgitating compartment, the total endocytic compartment open to regurgitation is progressively equilibrating, reaching a steady-state after ~30 min, in which the fraction of releasable HRP remains constant. If the chase was performed at 4°C, HRP loss was ~2%, confirming that HRP released at 37°C originated from an intracellular compartment.

The plateau attained after ~50 min suggests that after this time, HRP has either left an endocytic compartment by regurgitation, or was sequestered en route to a degradative compartment. The exponential parameter (see Appendix), deduced from regurgitation at equilibrium, is 0.053/min (Table III). In other words, ~5.3% of the endocytic compartment open to regurgitation was filled by endocytosed fluid every minute. The sum of HRP activity regurgitated and remaining inside the cells at all time points was 98 ± 13% of the value at the beginning of the chase, indicating that degradation could be neglected in these experiments.

Fluid-phase endocytosis rate can be estimated as the sum of accumulation and regurgitation rates. When normalized to an extracellular HRP concentration of 1 mg/ml, the rate of regurgitation at equilibrium, estimated by the initial slope of HRP release after 30- or 60-min pulse, amounted to 106 ± 14 ng/h/mg cell protein. Adding the rate of HRP accumulation at the same concentration after ⩾30 min (155 ± 19 ng/h/mg cell protein) yields the estimation of fluid-phase endocytosis in control cells at 261 ± 13 ng or nl/h/mg cell protein, a value very close to the direct measurement using short pulses, as described above (Table II).

Table II. Estimation of Fluid-phase Endocytosis

	Control	−KCl	NaCl 0.35 M
Short pulses (1–4 min)	267 ± 44	292 ± 59	198 ± 39
Long pulses (15–240 min)	261 ± 13	281 ± 29	252 ± 11

Results are values of clearance (equivalent extracellular volume cleared of HPR at a concentration of 1 mg/ml), in nl/h/mg cell protein.

Same material and experimental protocol as for Figs. 3 and 4. Values are mean ± SD of 6 to 12 dishes, compiled from two to three experiments. For long pulses, values represent the sum of accumulation and regurgitation rates at equilibrium.

Table III. Parameters and Accuracy of Kinetics of Fluid and Membrane Endocytic Filling

Experiment	Control		−KCl	
	k_f or k_{mb}	half-life	k_f or k_{mb}	half-life
	min^{-1}	*min*	*min*$^{-1}$	*min*
Fluid-phase tracer				
HRP regurgitation (30-60 min pulse)	0.053 ± 0.014	13.0	0.104 ± 0.018	6.7
Membrane tracers				
C6-NBD-GlcCer accumulation	0.058 ± 0.014	12.0	0.062 ± 0.022	11.2
TMA-DPH accumulation	0.059 ± 0.013	11.7	0.072 ± 0.019	9.6
C6-NBD-GlcCer recycling	0.065 ± 0.008	10.7	0.068 ± 0.010	10.2

Same material and experimental protocols as for Figs. 4, 5, and 6. k_f is the fraction of volume and k_{mb} is the fraction of membrane area labeled per min, according to Eq. A1, A2, and A3 (see Appendix). Results were obtained by nonlinear least squares fitting and are estimates ±asymptotic standard error.

For potassium depletion and hypertonicity, the HRP releasable fraction was increased approximately twofold compared to control cells: 69% after a 5-min pulse (Fig. 4 *a*), and 60% after a 15-min pulse (Fig. 4 *b*). As in control cells, a steady-state was also observed for pulses ⩾30 min, at which the HRP releasable fraction was 45% for potassium-depleted cells and 35% for NaCl-treated cells (Fig. 4 *c*). The corresponding exponential parameters at equilibrium indicate that ~11% of the available endocytic compartment open to regurgitation was filled with endocytosed fluid every minute in perturbed cells (Table III). Regurgitation at equilibrium, estimated by the initial slope of HRP release after 30- or 60-min pulses, amounted to 192 ± 35 ng/h/mg cell protein. As a consequence, the corrected measurement of fluid-phase endocytosis is very close to that of the control cells (266 ± 41 ng/h/mg cell protein, Table II). Hence, the twofold decrease of HRP intracellular accumulation after uptake >5 min observed in treated cells, could be fully accounted for by a comparable increase of regurgitation.

Since fluid-phase endocytosis was maintained in cells when the clathrin-dependent endocytosis was severely inhibited, we next focused on the effects of potassium depletion on the membrane endocytic traffic.

Membrane Endocytosis

Membrane endocytosis was estimated by the internalization and recycling of two fluorescent probes (for reviews see 23, 67). The glucosphingolipid derivative C6-NBD-GlcCer inserts into the outer leaflet of the plasma membrane and can be removed by back-exchange with BSA. The second probe, TMA-DPH, becomes fluorescent when inserted into lipid membranes and can be removed simply by phase partition in an aqueous medium. The usefulness of these two probes to study endocytosis has been established (24, 28), and provided similar measurements in rat foetal fibroblasts.

Both tracers showed an initial internalization efficiency of ~1% per min. Both in control and potassium-depleted cells, a steady-state was reached after 60 min when ~21% of the tracer was found intracellular and 79% at the cell surface (Fig. 5). This steady-state represents the equilibrium between membrane internalization and recycling. Mathematical analysis indicates that ~6–7% of the available endosomal membrane pool was filled every min by the plasma membrane lipid derivatives (Table III).

We next followed membrane recycling with C6-NBD-GlcCer (Fig. 6). No difference was observed between control and potassium-depleted cells. The corresponding exponential parameters indicate that ~6.6% of the available membrane of endosomes were replaced every minute in control and potassium-depleted cells (Table III); these param-

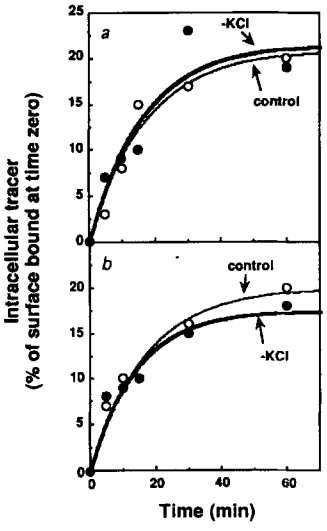

Figure 5. Effect of potassium depletion on membrane tracers accumulation. (*a*) C6-NBD-GlcCer. Control (*open circles*) and potassium depleted-cells (*filled circles*) were labeled at 4°C with 1 μM C6-NBD-GlcCer and incubated at 37°C in the appropriate simplified medium without BSA for the indicated times. Finally, cells were submitted to a back-exchange procedure at 4°C and lysed. The 100% values (tracer bound to the surface plasma membrane at 4°C) were ~1 nmol/mg cell protein, both in control and treated cells. (*b*) TMA-DPH. Control (*open circles*) and potassium depleted-cells (*filled circles*) were labeled at 4°C with 2 μM TMA-DPH and incubated at 37°C in the appropriate simplified medium for the indicated times. Finally, cells were washed at 4°C five times with PBS-Ca^{2+} and immediately assayed for fluorescence, as described in Materials and Methods. The 100% values were measured after 2 min cell labeling in PBS-Ca^{2+} for control cells and in 155 mM NaCl/2 mM $CaCl_2$ for potassium depleted-cells. Results are expressed as the percentages of lipid derivative internalized at 37°C, with respect to membrane-bound tracer at 4°C, as a function of the time. Residual value remaining after back-exchange for a 0 min incubation at 37°C was subtracted from all results (6% for C6-NBD-GlcCer and 2% for TMA-DPH). Each value is the mean of four dishes, with variation coefficient between 2 and 19%. These experiments were repeated once with similar results. Curves represent least squares fitting, according to equation A2 (see Appendix).

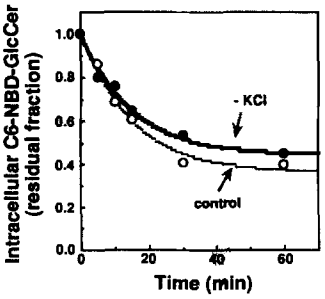

Figure 6. Effect of potassium depletion on C6-NBD-GlcCer recycling. Control (*open circles*) and potassium depleted-cells (*filled circles*) were labeled at 4°C with 1 μM C6-NBD-GlcCer and incubated for 60 min at 37°C in the appropriate simplified medium without BSA. Cells were then submitted to a back-exchange procedure at 4°C. After a second reincubation at 37°C for the indicated times in appropriate simplified medium, cells were transferred again at 4°C, submitted to a second back-exchange procedure and lysed. The experiment was repeated once with similar results. Each value is the mean of four dishes, with variations between 2 and 11%. The 100% values correspond to 230 pmol/mg cell protein. Curves represent least squares fitting, according to equation A3 (see Appendix).

eters are quite similar to those estimated from the internalization experiments (see above). These results indicate that increased HRP regurgitation in potassium-depleted cells is not due to any increase in the total amount of membrane recycled.

The fact that bulk fluid and membrane endocytic traffic were not affected by the treatment suggested that the size of primary endocytic vesicles in control and treated cells would be quite similar.

Analysis of Early Structures Involved in Fluid-phase Endocytosis

Very short pulses of HRP uptake (15–30 s) were used to identify by electron microscopy the primary structures responsible for fluid-phase endocytosis. In control cells, HRP cytochemistry resulted in labeling of both clathrin-coated and non-clathrin-coated vesicles (Fig. 7, *a–d*). Non-clathrin-coated vesicles corresponded either to endocytic vesicles that had lost their clathrin coat, to primary vesicles of a clathrin-independent pathway, or to structures of the recycling pathway. The latter possibility seemed unlikely in view of the short duration of the pulses (15–30 s), and because only small vesicles were fully labeled, while very few endosomes were slightly labeled in these control cells. Primary endocytic vesicles could rapidly (after 30 to 60 s) fuse with each other (Fig. 7 *c*) or with preexisting peripheral endosomes, where HRP was diluted (Fig. 7 *d*), as described by Griffiths et al. (15).

Short pulses of HRP uptake (15–30 s) in potassium-depleted cells resulted in labeling of numerous small non-clathrin-coated vesicles (Fig. 7 *e*) and thereafter of larger endosomes.

Because the identification of the clathrin coat was frequently questionable, due to some diffusion of the peroxidase reaction product, the size distribution of all HRP-labeled vesicles was analyzed in control and treated cells after a 15-s pulse, when there were essentially primary endocytic labeled vesicles. In control cells, the size distribution of HRP-labeled particles was superposable to that of clathrin-coated particles (Fig. 8 *a*). Moreover, the size distribution of HRP-labeled particles after potassium depletion was indistinguishable from that of control cells (Fig. 8 *b*).

Discussion

Efficiency and Mechanism of Inhibition of Receptor-mediated Endocytosis

Intracellular potassium depletion and incubation of rat foetal fibroblasts in a moderately hypertonic medium both produce a severe (~−90%) and reversible inhibition of receptor-mediated endocytosis, although internalization of receptor-bound transferrin is not fully blocked. In parallel, the total membrane area of clathrin-coated pits and peripheral coated profiles is decreased to a similar extent. A first explanation is that formation of clathrin-coated endocytic vesicles is not fully arrested and that clathrin polymerization could be rate-limiting for receptor-mediated endocytosis. We have however no evidence that the smaller and less abundant clathrin-coated pits that are still detected in perturbed cells are competent for endocytosis.

Alternatively, since both perturbations do not affect endocytosis of membrane lipid derivatives, transferrin-receptor complexes could be no longer concentrated in the endocytic pits and merely follow the bulk membrane flow. Indeed, clathrin-coated pits concentrate transferrin receptor about 10-fold (17), and conversely, truncated receptors lacking the cytoplasmic domain comprising specific sequences for concentration in clathrin-coated pits and for rapid endocytosis are still internalized at a ~10-fold lower rate (~1% of surface pool per min), corresponding to bulk membrane flow (69).

The mechanism of inhibition of receptor-mediated endocytosis by the two procedures used here is still elusive. Potassium depletion and incubation in hypertonic medium have pleiotropic, partially overlapping effects. In particular, both treatments somehow cause abnormal polymerization of clathrin as empty microcages. Conceivably, this would deplete the cytosolic pool of soluble clathrin and prevent its recruitment into newly formed endocytic pits, while the AP2 complexes can still be detected at the plasma membrane (18, 20, 21).

Fluid-phase Endocytosis

A reliable measurement of fluid-phase endocytosis is not trivial (70). Moreover, except for very short pulses that are not technically easy to perform, net accumulation of tracer underestimates fluid-phase endocytosis due to vesicular regurgitation, the proportion of which varies among cell types (4). It is reassuring to note that in control rat foetal fibroblasts, as well as in potassium-depleted and NaCl-treated cells, quite similar estimates were obtained, either by direct measurement of accumulation after short pulses, or by the sum of accumulation and regurgitation after longer pulses at steady-state.

In control fibroblasts, regurgitation is suggested by a decline in the rate of HRP accumulation at ~5 min and its measured rate (106 ± 14 nl/h/mg cell protein) represents a significant part of the initial clearance by fluid-phase endocytosis (261 ± 13 nl/h/mg cell protein). Computations show that the lower subsequent accumulation of the fluid-phase tracer in treated cells for pulses >5 min can be fully accounted for by enhancement of regurgitation. It can thus be speculated that the unequal decrease of fluid-phase endocytosis tracer accumulation observed in various cell types, upon blockage of the clathrin-associated pathway (11, 16, 32,

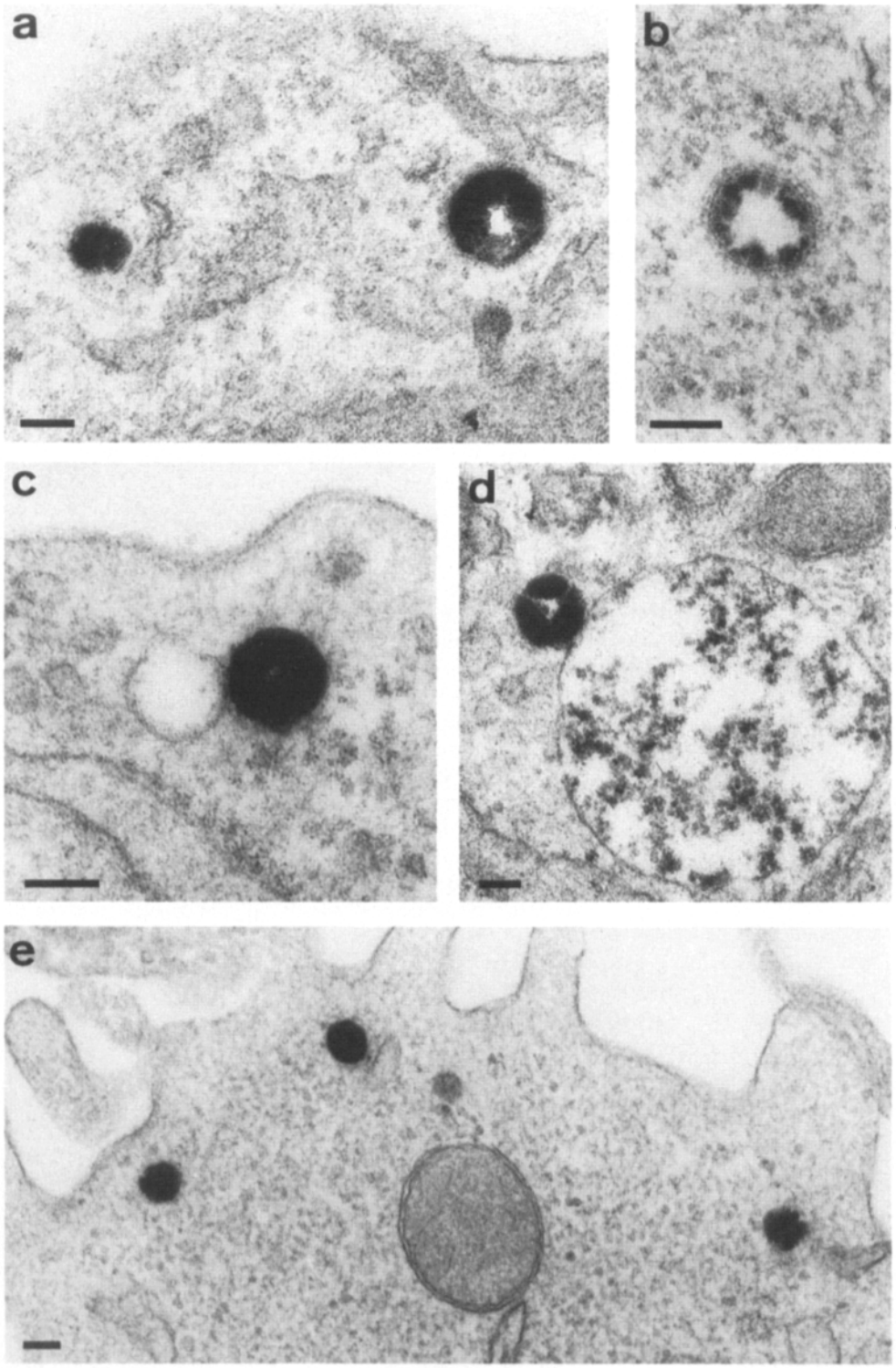

Figure 7. Early structures involved in HRP endocytosis. Control and potassium-depleted cells were incubated at 37°C for very short intervals in the corresponding simplified medium, containing 8 mg/ml HRP. They were immediately cooled at 4°C, washed extensively and fixed with 2% glutaraldehyde at 4°C. HRP activity was demonstrated with diaminobenzidine and H_2O_2 in the presence of 25 mM merthiolate. (*a–d*) Control cells. (*a*) The small profile at left is noncoated and the larger profile at right is coated, ~15-s pulse; (*b*) the clathrin coat is better evidenced with less developed cytochemistry, ~15-s pulse; (*c*) pending fusion between noncoated vesicular profiles, one containing HRP and the other not, ~30-s pulse; (*d*) fusion between a labeled vesicle without detectable clathrin coat and an endosome, where the label is apparently diluted, ~90-s pulse; (*e*) potassium-depleted cell showing three non-clathrin-coated vesicular profiles of similar diameter, ~15-s pulse. Bars, 100 nm.

40, 41, 49), reflects a corresponding stimulation of tracer regurgitation, possibly by induction of rab4 recruitment (64).

Membrane Endocytosis

Membrane traffic analysis in control and treated cells, using the two lipid derivatives C6-NBD-GlcCer and TMA-DPH, revealed identical endocytic kinetics and steady-state values. At equilibrium between internalization and recycling, about 20% of labeled membrane lipids reside within the cell, as compared with the cell surface. This value is very close to that found in other cells with lipid derivatives (24, 28), or with surface glycoconjugates (7). These levels are also in excellent agreement with morphometrical estimations on the respective contribution of the endosomal and pericellular membrane pool in BHK cells (15).

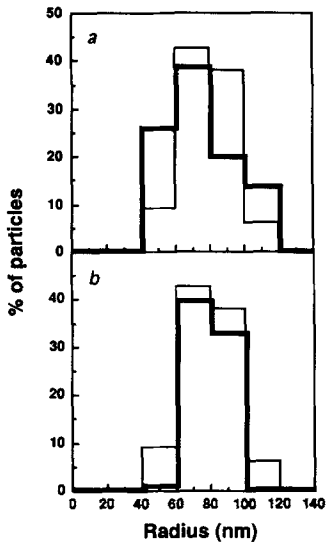

Figure 8. Size distribution of HRP-labeled early endocytic structures in control and potassium-depleted cells. Same protocol as for Fig. 7. All labeled profiles after 15 s of HRP uptake were photographed (99 and 69 for control and potassium-depleted cells, respectively) and size distribution of particles was determined as in Fig. 2. Based on the clathrin-coated particle size distribution, particles with a radius higher than 140 nm were assumed to represent endosomes and were excluded from the representation (see also 16). The upper panel compares the size distribution in control cells of HRP-labeled particles (*thin line*) and clathrin-coated particles (*thick line*, reproduced from Fig. 2). The lower panel compares the size distribution of HRP-labeled profiles in control (*thin line*) and potassium-depleted cells (*thick line*).

The biochemical measurement of recycling of C6-NBD-GlcCer is similar to that of transferrin (data not shown) in control rat foetal fibroblasts ($t_{1/2}$ of ~11 min). This value is also very close to those deduced using a morphological approach for *N*-[*N*-(7-nitro-2,1,3-benzoxadiazol-4-yl)-ε-aminohexanoyl]-sphingosylphosphorylcholine (C6-NBD-SM) and transferrin, and thus support the model of bulk flow recycling of membrane constituents such as the transferrin receptor (36). Colocalization of transferrin and C6-NBD-GlcCer during early stage of endocytosis and recycling has also been shown in BHK cells (28).

C6-NBD-GlcCer and TMA-DPH accumulate and recycle in potassium-depleted cells with kinetics indistinguishable from that of control cells. This indicates that these probes are not specifically concentrated into clathrin-coated pits. In addition, potassium depletion has different effects on fluid regurgitation and membrane recycling. We have observed that this perturbation results in enlarged and more peripherally located peroxidase-labeled endosomes, and severely inhibits the transfer of internalized peroxidase into dense lysosomes as followed by analytical subcellular fractionation (our unpublished observations). Taken together, an increase of the volume/surface ratio of endosomes, combined with a block of the transfer of fluid-phase tracer from the early endocytic, readily regurgitating, endosomes, to a later, more sequestrating compartment, provides a reasonable explanation for the enhanced regurgitation of fluid without appreciable effect on membrane lipid recycling. This interpretation is fully in agreement with the generally held model in which the bulk of internalized membrane is recycled, while a comparably much larger fraction of internalized fluid is normally transferred to lysosomes (e.g., 10).

Another glucosylceramide, *N*-[5-(5,7-dimethyl BODIPY™)-1-pentanoyl]-glucosylsphingosine (C5-DMB-GlcCer), has recently been shown to enter by an endocytic and a nonendocytic pathway in established human skin fibroblasts (35). However, internalization of C6-NBD-GlcCer in rat foetal fibroblasts by a nonendocytic pathway, if any, can be neglected, since the back-exchange procedure allows to remove 94% of the tracer initially bound to the cell surface at 4°C. This level is comparable to those obtained in established human skin fibroblasts for two other probes that are internalized only (C5-DMB-sphingosylphosphorylcholine) or mostly (C5-DMB-galactosylceramide) by an endocytic pathway (35). In addition, studies of C6-NBD-GlcCer internalization failed to detect a nonendocytic pathway for this probe in BHK cells (28). Finally, the internalization kinetics of C6-NBD-GlcCer in rat foetal fibroblasts is very similar to that of TMA-DPH, a tracer only entering by endocytosis (24), and is in good agreement with that of membrane glycoconjugates (7).

Nature of the Clathrin-independent Pinocytic Pathway

The fact that fluid and membrane internalizations are not affected in rat foetal fibroblasts when formation of clathrin-coated pits is severely inhibited establishes the existence of a clathrin-independent endocytic pathway in the perturbed cells. We will now examine its structural counterpart and evaluate the relevance of the observations to untreated cells.

(*a*) A first hypothesis is that a distinct clathrin-independent endocytic pathway is induced or stimulated in treated cells, possibly by enhanced recruitment of rab5 (6, 38, 71), so as to compensate for the loss of the clathrin-associated pathway. However, the regulatory mechanism that would maintain the total endocytic traffic of fluid and membrane constant in the presence or absence of clathrin-associated endocytosis remains totally unclear. Based on the indistinguishable average diameter of endocytic clathrin-coated pits/vesicles and of HRP-labeled primary endocytic vesicles, as well as the identical rates of fluid and membrane endocytosis, in control and perturbed cells, implying identical volume/surface ratios, it can be concluded that clathrin-independent endocytosis is supported by primary vesicles with a diameter of ~150 nm. This conclusion excludes caveolae and macropinocytic vesicles. It is also in good agreement with the very close diameters of clathrin-coated and clathrin-independent primary endocytic pits/vesicles in HEp-2 cells, although no stimulation of the clathrin-independent pathway was observed after potassium depletion in these cells (16).

(*b*) However, our data are also entirely consistent with the possibility that clathrin is not an essential component for the invagination and budding machinery, but is required for the specific enrichment of some plasma membrane proteins mediated by interaction with AP2 complexes. The machinery responsible for invagination and budding would not be perturbed by the two treatments, and accordingly, the traffic of fluid and membrane would remain unaffected. This unifying hypothesis, that we favor, does not exclude that pinocytic pits and vesicles, decorated or not by clathrin, can coexist in normal cells.

In isolated rat hepatocytes, hypertonicity blocks receptor-mediated endocytosis of asialo-orosomucoid, but does not affect fluid-phase uptake of Lucifer Yellow (40). This result was regarded as evidence for two distinct endocytic pathways, but is also compatible with our hypothesis, which explains more easily the necessary participation of coated pits to pinocytosis and the identical activation energy required for receptor-mediated and fluid-phase endocytosis (41).

Genetic depletion of clathrin heavy chain led to apparently opposite effects. *Saccharomyces cerevisiae*, mutated in the clathrin heavy chain gene, still internalized α-factor to 30–50% of wild type (43, 58). This could indicate that clathrin is a dispensable driving force for formation and budding of endocytic vesicles, but not for clustering of receptors. In contrast, antisense depletion of the clathrin heavy chain mRNA in *Dictyostelium discoideum* led to a ~85% decrease of fluid-phase tracer accumulation (39). Whether regurgitation was also affected was not reported.

If clathrin is not an essential constituent for the vesiculation machinery, which could be the candidate? The budding of clathrin-coated vesicles requires ATP hydrolysis and several specific cytosolic factors (51), including the GTP-binding protein dynamin (52, 62). Interestingly, overexpressing dynamin mutated in its GTP-binding site affects an early step of pit invagination and blocks transferrin endocytosis (19, 63). However, the effects of mutated dynamin on fluid-phase endocytosis are contradictory, since it is blocked in *shibire*-derived tissues or cell lines (29, 60), but preserved in transfected COS-7 cells (19).

In conclusion, results presented here show that the conceptual problem of pinocytosis without clathrin is either to consider that clathrin-dependent or -independent endocytosis are distinct phenomena, with separate structures and molecular mechanisms, or to consider that pinocytic pits and vesicles can be decorated or not by clathrin, that provides enrichment of some membrane constituents. Until this controversy is solved, we prefer to refer to bulk pinocytosis as either clathrin-associated or non–clathrin-associated phenomena.

Appendix

Mathematical Modeling of Fluid and Membrane Tracers Kinetics

Fluid Regurgitation. Our model for endocytosis assumes that tracers of fluid-phase endocytosis, such as HRP, converge to an endosomal compartment from which they can be either released without any modification in the extracellular medium, or directed to a degradative pathway. Since the sum of released and cell-associated HRP activities are constant and since half-life for degradation of HRP, once in lysosomes, is ~5 h, digestion of this tracer can be neglected (unpublished observations). The chase period is characterized by an exponential HRP release, due to dilution of the tracer in the endocytic compartment participating to regurgitation by incoming fluid devoid of HRP. The plateau indicates that remaining intracellular HRP has been sequestered in a degradative compartment. Regurgitation of fluid-phase tracers after accumulation can be described by the following equation:

$$\frac{Q_t}{Q_o} = 1 - \frac{Q_r}{Q_o}(1 - e^{-k_f t}) \quad \text{(A1)}$$

in which: Q_t is the amount of intracellular tracer at time t (ng/mg cell protein); Q_o is the amount of intracellular tracer at the beginning of the chase (ng/mg cell protein); Q_r is the maximal amount of releasable tracer (ng/mg cell protein); k_f is the exponential filling rate by the fluid tracer of the endocytic compartment participating to regurgitation (min^{-1}); t is the time (min).

Membrane Internalization. Our model further assumes that membrane tracers, such as C6-NBD-GlCer or TMA-DPH, progressively equilibrate by lateral diffusion and by mixing with an internal membrane pool. As shown in rat foetal fibroblasts, import from plasma membrane to the lysosomes can be neglected for the time-scale of our experiments (12). A steady-state is reached, where endocytic and exocytic labeled membrane traffic are in equilibrium. Membrane internalization is characterized by the following equation:

$$\frac{Q_i}{Q_p} = \frac{S_i}{S_p}(1 - (1 - e^{-k_{mb}t}) \quad \text{(A2)}$$

in which: Q_i is the amount of intracellular membrane-tracer (ng/mg cell protein); Q_p is the amount of plasma membrane-tracer at 4°C (ng/mg cell protein); S_i and S_p are the endosomal and plasma membrane surfaces, respectively (cm^2/mg cell protein); k_{mb} is the exponential filling rate by the membrane tracer of the recycling compartment (min^{-1}); t is the time (min).

Membrane Recycling. In pulse-chase experiments, membrane recycling induces an exponential tracer release, owing to the dilution of labeled endosomal membrane by incoming unlabeled membrane. This process can be described by an equation similar to equation A1:

$$\frac{Q_t}{Q_o} = 1 - \frac{Q_r}{Q_o}(1 - e^{-k_{mb}t}) \quad \text{(A3)}$$

in which Q_t, Q_o, Q_r, and t have the same meaning as for equation (A1) and k_{mb} has the same meaning as for equation (A2). Membrane internalization and recycling analysis thus yield independent estimates of k_{mb} and hence of the half-life.

In the present study, average values were adjusted to the exponential function (equation A1, A2, and A3), by least squares nonlinear fitting. Fitting was performed with a SYSTAT program, version 5.2 (SYSTAT Inc., Evanston, IL), on a Macintosh IIci computer.

We wish to thank Ms. N. Delflasse, T. Lac, M. Leruth, and F. N'Kuli for their excellent technical assistance. We are especially grateful to Professors D. Hoekstra and J.-G. Kuhry for kindly providing lipids probes and advice. The critical comments on this manuscript by Drs. G. Griffiths, D. Hoekstra, J.-G. Kuhry, B. Van Deurs, C. Watts, and M. Zerial are particularly appreciated. P. J. Courtoy wants to dedicate this work to G. K., L. T., and C. W. and to the memory of Eric Holtzman.

P. Cupers and A. Veithen were supported in part by a training grant of the Institut pour l'encouragement de la Recherche Scientifique en Industrie et en Agriculture (Belgium) and also by the University of Louvain for P. Cupers. Professor A. L. Kiss was supported by the International Institute of Cellular and Molecular Pathology. These investigations were covered by grants 3.4570.88, 2.4588.93, 3.4603.93 and 7.4547.93 of the Belgian National Fund for Scientific Research, as well as by the Belgian State (Primer Minister's Office) Science Policy Programming (Concerted Actions) and Framework of Interuniversity Attraction Pole.

Received for publication 2 May 1994 and in revised form 19 July 1994.

References

1. Anderson, R. G. W. 1993. Plasmalemmal caveolae and GPI-anchored membrane proteins. *Curr. Opin. Cell Biol.* 5:647–652.
2. Bar-Sagi, D., and J. R. Feramisco. 1986. Induction of membrane ruffling and fluid-phase pinocytosis in quiescent fibroblasts by ras proteins. *Science (Wash. DC).* 233:1061–1068.
3. Bergmeyr, H. U., and E. Bernt. 1972. *In* Methods of Enzymatic Analysis. Vol 2. H. U. Bergmeyr, editor. Academic Press Inc., NY. 574–579.
4. Besterman, J. M., J. A. Airhart, R. C. Woodworth, and R. B. Low. 1981. Exocytosis of pinocytosed fluid in cultured cells: kinetic evidence for rapid turnover and compartmentation. *J. Cell Biol.* 91:716–727.
5. Blomhoff, R., M. S. Nenseter, M. H. Green, and T. Berg. 1989. A multicompartmental model of fluid-phase endocytosis in rabbit liver parenchymal cells. *Biochem. J.* 262:605–610.
6. Bucci, C., R. G. Parton, I. H. Mather, H. Stunnenberg, K. Simons, B. Hoflack, and M. Zerial. 1992. The small GTPase Rab5 functions as a regulatory factor in the early endocytic pathway. *Cell.* 70:715–728.
7. Burgert, H.-G., and L. Thilo. 1983. Internalization and recycling of plasma membrane glycoconjugates during pinocytosis in the macrophages cell line P388D1. *Exp. Cell Res.* 144:127–142.
8. Conway, E. M., B. Nowakowski, and M. Steiner-Mosonyi. 1994. Thrombomodulin lacking the cytoplasmic domain efficiently internalizes thrombin via nonclathrin-coated, pit-mediated endocytosis. *J. Cell Physiol.* 158:285–298.
9. Cosson, P., I. de Curtis, J. Pouysségur, G. Griffiths, and J. Davoust. 1989. Low cytoplasmic pH inhibits endocytosis and transport from the *trans*-Golgi network to the cell surface. *J. Cell Biol.* 108:377–387.
10. Courtoy, P. J. 1991. Dissection of endosomes. *In* Intracellular Trafficking of Proteins. C. S. Steer and J. A. Hanover editors. Cambridge University Press. 103–156.
11. Daukas, G., and S. H. Zigmond. 1985. Inhibition of receptor-mediated but not fluid-phase endocytosis in polymorphonuclear leukocytes. *J. Cell Biol.* 101:1673–1679.
12. Draye, J.-P., P. J. Courtoy, J. Quintart, and P. Baudhuin. 1988. A quantitative model of traffic between plasma membrane and secondary lysosomes: evaluation of inflow, lateral diffusion, and degradation. *J. Cell Biol.* 107:2105–2115.

13. Dupree, P., R. G. Parton, G. Raposo, T. V. Kurzchalia, and K. Simons. 1993. Caveolae and sorting in the trans Golgi network of epithelial cells. *EMBO (Eur. Mol. Biol. Organ.) J.* 12:1597–1605.
14. Fire, E., D. E. Zwart, M. G. Roth, and Y. I. Henis. 1991. Evidence from lateral mobility studies for dynamic interactions of a mutant influenza hemagglutinin with coated pits. *J. Cell Biol.* 115:1585–1594.
15. Griffiths, G., R. Back, and M. Marsh. 1989. A quantitative analysis of the endocytic pathway in baby hamster kidney cells. *J. Cell Biol.* 109: 2703–2720.
16. Hansen, S. H., K. Sandvig, and B. Van Deurs. 1991. The preendosomal compartment comprises distinct coated and noncoated endocytic vesicle populations. *J. Cell Biol.* 113:731–741.
17. Hansen, S. H., K. Sandvig, and B. Van Deurs. 1992. Internalization efficiency of the transferrin receptor. *Exp. Cell Res.* 199:19–28.
18. Hansen, S. H., K. Sandvig, and B. Van Deurs. 1993. Clathrin and HA2 adaptors: effects of potassium depletion, hypertonic medium and cytosol acidification. *J. Cell Biol.* 121:61–72.
19. Herskovits, J. S., C. C. Burgess, R. A. Obar, and R. B. Vallee. 1993. Effects of mutant rat dynamin on endocytosis. *J. Cell Biol.* 122:565–578.
20. Heuser, J. 1989. Effect of cytoplasmic acidification on clathrin lattice morphology. *J. Cell Biol.* 108:401–411.
21. Heuser, J. E., and R. G. W. Anderson. 1989. Hypertonic media inhibit receptor-mediated endocytosis by blocking clathrin-coated pit formation. *J. Cell Biol.* 108:389–400.
22. Hewlett, L. J., A. R. Prescott, and C. Watts. 1994. The coated pit and macropinocytic pathways serve distinct endosome populations. *J. Cell Biol.* 124:689–703.
23. Hoekstra, D., and J. W. Kok. 1992. Trafficking of glycosphingolipids in eukaryotic cells; sorting and recycling of lipids. *Biochem. Biophys. Acta.* 1113:277–294.
24. Illinger, D., and J.-G. Kuhry. 1994. The kinetic aspects of intracellular fluorescence labelling with TMA-DPH support the maturation model for endocytosis in L929 cells. *J. Cell Biol.* 125:783–794.
25. Ilondo, M. M., J. Smal, P. De Meyts, and P. J. Courtoy. 1991. Comparison of the effects of hypertonic sucrose and intracellular potassium depletion on growth hormone receptor binding kinetics and down-regulation in IM-9 cells: evidence for a sequential block of receptor-mediated endocytosis. *Endocrinology.* 128:1597–1602.
26. Keen, J. H. 1990. Clathrin and associated assembly and disassembly proteins. *Annu. Rev. Biochem.* 59:415–438.
27. Keller, H. U. 1990. Diacylglycerols and PMA are particularly effective stimulators of fluid pinocytosis in human neutrophils. *J. Cell Physiol.* 145:465–471.
28. Kok, J. W., K. Hoekstra, S. Eskelinen, and D. Hoekstra. 1992. Recycling pathways of glucosylceramide in BHK cells: distinct involvement of early and late endosomes. *J. Cell Sci.* 103:1139–1152.
29. Kosaka, T., and K. Ikeda. 1983. Reversible blockage of membrane retrieval and endocytosis in the Garland cell of the temperature-sensitive mutant of *Drosophila melanogaster, shibire. J. Cell Biol.* 97:499–507.
30. Larkin, J. M., M. S. Brown, J. L. Goldstein, and R. G. W. Anderson. 1983. Depletion of intracellular potassium arrests coated pit formation and receptor-mediated endocytosis in fibroblasts. *Cell.* 33:273–285.
31. Madshus, I. H., T. I. Tonnessen, S. Olsnes, and K. Sandvig. 1987. Effect of potassium depletion of HEp-2 cells on intracellular pH and on chloride uptake by anion antiport. *J. Cell Physiol.* 131:6–13.
32. Madshus, I. H., K. Sandvig, S. Olsnes, and B. Van Deurs. 1987. Effect of reduced endocytosis by hypotonic choc and potassium depletion on the infection of HEp-2 cells by picornavirus. *J. Cell Physiol.* 131:14–22.
33. McFarlane, A. S. 1958. Efficient trace-labeling of proteins with iodine. *Nature (Lond.).* 183:53.
34. Marsh, M., and A. Helenius. 1980. Adsorptive endocytosis of Semliki forest virus. *J. Mol. Biol.* 142:439–454.
35. Martin, O. C., and R. E. Pagano. 1994. Internalization and sorting of a fluorescent analogue of glucosylceramide to the Golgi apparatus of human skin fibroblasts: utilization of endocytic and nonendocytic transport mechanisms. *J. Cell Biol.* 125:769–781.
36. Mayor, S., J. F. Presley, and F. R. Maxfield. 1993. Sorting of membrane components from endosomes and subsequent recycling to the cell surface occurs by a bulk flow process. *J. Cell Biol.* 121:1257–1269.
37. Moya, M., A. Dautry-Varsat, B. Goud, D. Louvard, and P. Boquet. 1985. Inhibition of coated pit formation in HEp-2 cells blocks the cytotoxicity of diphtheria toxin but not that of ricin toxin. *J. Cell Biol.* 101:548–559.
38. Novick, P., and P. Brennwald. 1993. Friends and family: the role of the Rab GTPases in vesicular traffic. *Cell.* 75:597–601.
39. O'Halloran, T. J., and R. G. W. Anderson. 1992. Clathrin heavy chain is required for pinocytosis, the presence of large vacuoles and development in *Dictyostelium. J. Cell Biol.* 118:1371–1377.
40. Oka, J. A., M. D. Christensen, and P. H. Weigel. 1989. Hypertonicity inhibits galactosyl receptor-mediated but not fluid-phase endocytosis in isolated rat hepatocytes. *J. Biol. Chem.* 264:12016–12024.
41. Oka, J. A., and P. H. Weigel. 1989. The pathways for fluid-phase and receptor-mediated endocytosis in rat hepatocytes are different but thermodynamically equivalent. *Biochem. Biophys. Res. Commun.* 159: 488–494.
42. Parton, R. G., C. D. Ockeford, and D. R. Critchley. 1988. Tetanus toxin binding to mouse spinal cord cells: an evaluation of the role of gangliosides in toxin internalization. *Brain Res.* 475:118–127.
43. Payne, G. S., D. Baker, E. Van Tuinen, and R. Schekman. 1988. Protein transport to the vacuole and receptor-mediated endocytosis by clathrin heavy chain-deficient yeast. *J. Cell Biol.* 106:1453–1461.
44. Pearse, B. M. F., and M. S. Robinson. 1990. Clathrin, adaptors and sorting. *Annu. Rev. Cell Biol.* 6:151–171.
45. Prill, V., L. Lehmann, K. Von Figura, and C. Peters. 1993. The cytoplasmic tail of lysosomal acid phosphatase contains overlapping but distinct signals for basolateral sorting and rapid internalization in polarized MDCK cells. *EMBO (Eur. Mol. Biol. Organ.) J.* 12:2181–2193.
46. Racoosin, E. L., and J. A. Swanson. 1993. Macropinosome maturation and fusion with tubular lysosomes in macrophages. *J. Cell Biol.* 121: 1011–1020.
47. Raposo, G., I. Dunia, C. Delavier-Klutchko, S. Kaveri, A. D. Strosberg, and E. L. Benedetti. 1989. Internalization of β-adrenergic receptor in A431 cells involves non-coated vesicles. *Eur. J. Cell Biol.* 50:340–352.
48. Rothberg, K. G., J. E. Heuser, W. C. Donzell, Y.-S. Ying, J. R. Glenney, and R. G. W. Anderson. 1992. Caveolin, a protein component of caveolae membrane coats. *Cell.* 68:673–682.
49. Sandvig, K., S. Olsnes, O. W. Petersen, and B. Van Deurs. 1987. Acidification of the cytosol inhibits endocytosis from coated pits. *J. Cell Biol.* 105:679–689.
50. Sandvig, K., S. Olsnes, J. E. Brown, O. W. Petersen, and B. Van Deurs. 1989. Endocytosis from coated pits of Shiga toxin: a glycolipid-binding protein from *Shigella dysenteria* 1. *J. Cell Biol.* 108:1331–1343.
51. Schmid, S. L. 1993. Biochemical requirements for the formation of clathrin- and COP-related transport vesicles. *Curr. Opin. Cell Biol.* 5:621–627.
52. Shpetner, H. S., and R. B. Vallee. 1992. Dynamin is a GTPase stimulated to high levels of activity by microtubules. *Nature (Lond.).* 355:733–735.
53. Smart, E. J., D. C. Foster, Y.-S. Ying, B. A. Kamen, and R. G. W. Anderson. 1994. Protein kinase C activators inhibit receptor-mediated potocytosis by preventing internalization of caveolae. *J. Cell Biol.* 124: 307–313.
54. Smythe, E., and G. Warren. 1991. The mechanism of receptor-mediated endocytosis. *Eur. J. Biochem.* 202:689–699.
55. Sorkin, A., and G. Carpenter. 1993. Interaction of activated EGF receptors with coated pit adaptins. *Science (Wash. DC).* 261:612–615.
56. Steinman, R. M., S. E. Brodie, and Z. A. Cohn. 1976. Membrane flow during pinocytosis. *J. Cell Biol.* 68:665–687.
57. Swanson, J. A., B. D. Yirinec, and S. C. Silverstein. 1985. Phorbol esters and horseradish peroxidase stimulate pinocytosis and redirect the flow of pinocytosed fluid in macrophages. *J. Cell Biol.* 100:851–859.
58. Tan, P. K., N. G. Davis, G. F. Sprague, and G. S. Payne. 1993. Clathrin facilitates the internalization of seven transmembrane segment receptors for mating pheromones in yeast. *J. Cell Biol.* 123:1707–1716.
59. Tran, D., J. L. Carpentier, F. Sawano, P. Gorden, and L. Orci. 1987. Ligands internalized through coated or noncoated invaginations follow a common intracellular pathway. *Proc. Natl. Acad. Sci. USA.* 84: 7957–7961.
60. Tsuruhara, T., J. H. Koenig, and K. Ikeda. 1990. Synchronized endocytosis in the oocyte of a temperature-sensitive mutant of *Drosophila melanogaster. Cell Tissue Res.* 259:199–207.
61. Tulkens, P., H. Beaufays, and A. Trouet. 1974. Analytical fractionation of homogenates from cultured rat embryo fibroblasts. *J. Cell Biol.* 63:383–401.
62. Vallee, R. B., and H. S. Shpetner. 1993. Dynamin in synaptic dynamics. *Nature (Lond.).* 365:107–108.
63. Van Der Bliek, A. M., T. E. Redelmeier, H. Damke, E. J. Tisdale, E. M. Meyerowitz, and S. L. Schmid. 1993. Mutations in human dynamin block an intermediate stage in coated vesicle formation. *J. Cell Biol.* 122:553–563.
64. Van Der Sluijs, P., M. Hull, P. Webster, P. Male, B. Goud, and I. Mellman. 1992. The small GTP-binding protein Rab4 controls an early sorting event on the endocytic pathway. *Cell.* 70:729–740.
65. Van Deurs, B., O. W. Petersen, S. Olsnes, and K. Sandvig. 1989. The ways of endocytosis. *Int. Rev. Cytol.* 117:131–169.
66. Van Deurs, B., P. K. Holm, K. Sandvig, and S. H. Hansen. 1993. Are caveolae involved in clathrin-independent endocytosis? *Trends Cell Biol.* 3:249–251.
67. Van Meer, G. 1993. Transport and sorting of membrane lipids. *Curr. Opin. Cell Biol.* 5:661–673.
68. Vaux, D. 1992. The structure of an endocytic signal. *Trends Cell Biol.* 2:189–192.
69. Watts, C., and M. Marsh. 1992. Endocytosis: what goes in and how? *J. Cell Sci.* 103:1–8.
70. Wiley, H. S., and D. N. McKinley. 1987. Assay of growth factor stimulation of fluid-phase endocytosis. *Meth. Enzymol.* 146:402–417.
71. Zerial M., and H. Stenmark. 1993. Rab GTPases in vesicular transport. *Curr. Opin. Cell Biol.* 5:613–620.